# Atomistic Molecular Dynamics Simulation of Hexakis(pentyloxy)triphenylene: Structure and Translational Dynamics of Its Columnar State

**Giorgio Cinacchi,*,†,‡,§ Renato Colle,†,||,⊥ and Alessandro Tani‡,#**

*Scuola Normale Superiore, Piazza dei Cavalieri 7, I-56126 Pisa, Italy, Dipartimento di Chimica e Chimica Industriale, Universita di Pisa, Via Risorgimento 35, I-56126 Pisa, Italy, and Dipartimento di Chimica Applicata e Scienza dei Materiali, Universita di Bologna, Via Saragozza 8, I-40136 Bologna, Italy*

*Received: January 24, 2004; In Final Form: March 24, 2004*

Atomistic molecular dynamics computer simulations have been performed on the columnar state of the discogen hexakis(pentyloxy)triphenylene (HAT5). The parameters of the empirical model potential have been taken from the AMBER and OPLS force fields. A 10 ns simulation run has been carried out in Berendsen's ensemble at pressure $P = 0.1$ MPa and temperature $T = 375$ K to study bulk and molecular structure. The bulk structure has been characterized by obtaining structural parameters that compare favorably with those deduced from X-ray diffraction experiments. $^{13}C$ and $^{2}H$ NMR data suggest two completely different pictures of the position of the pendant chains with respect to the plane of the aromatic core: one, called *diablo-like*, with the chains in the triphenylene plane; the other, *octopus-like*, with the chains out of this plane and, alternatively, above and below it. Our simulated data are consistent with an intermediate situation. In agreement with all NMR data, we find that the chains become more and more disordered, moving away from the core. We have observed a decrease of the disorder of the lateral chains in going from gas phase to condensed bulk state. Information on translational dynamics has been obtained by performing a 1 ns simulation in the microcanonical ensemble; these calculations definitely assess the one-dimensional fluid character of the columnar state. We have found that the mean square displacement has a solidlike behavior in the plane perpendicular to the column axis. The translational dynamics along the direction parallel to it is dominated by the reciprocal, fluidlike sliding motion of the columns as a whole. If this collective dynamics is removed, also the parallel diffusion coefficient turns out to be solidlike.

## 1. Introduction

Discotic thermotropic liquid crystals are usually formed by flat molecules with a central aromatic core and several pendant aliphatic chains at its edges. Besides a discotic nematic phase ($N_D$), analogous to that found in calamitic (rodlike) mesogens, they give rise to a number of columnar phases (D), where the molecules stack on top of each other and the resulting columns are arranged in a regular lattice. Such columnar mesophases are classified in terms of: (i) the two-dimensional lattice, which can be hexagonal (h), rectangular (r) or oblique (ob); (ii) the one-dimensional organization inside each columnar array, which can be ordered (o) or disordered (d); (iii) the orientation of the main axis of the molecules with respect to the column axis.[1−6]

Among the discotic thermotropic liquid crystals, particular attention has been devoted to the members of the hexakis-(alkyloxy)triphenylenes (HAT*n*) homologue series, which exhibit columnar hexagonal ordered phases ($D_{ho}$) and can have interesting technological applications as one-dimensional conductors.[7−22] In Figure 1 we show the structure of the molecule, that is, the building block of the columns, and the experimental phase diagram, as a function of the number (*n*) of carbon atoms in the side chains.

The members of the HAT*n* series may be considered as prototypes of disklike mesogenic molecules and are among the first discogens synthesized after the discovery of these materials in 1977.[1] A number of experimental studies have been performed to elucidate aspects of their structure and dynamics,[23−33] but definite conclusions have not been drawn until now.

In this respect, computer simulation techniques offer a unique tool to improve our understanding of these mesophases at the molecular level, supporting and complementing the experimental work. The number of computer simulations so far performed on discotic materials is, however, relatively small. Most of them have used idealized model potentials to obtain a general understanding of the phase diagram,[34−39] but a closer contact with real experiments requires resorting to more realistic models with chemical detail. To our knowledge, only two simulation studies on bulk discotic thermotropic liquid crystals have been carried out employing an atomistic model: in ref 40, the molecular dynamics (MD) of an isotropic sample of 32 molecules of hexaheptanoate of benzene (BHA7) has been simulated for about 200 ps, whereas in ref 41 the MD of a sample of 54 HAT5 molecules, arranged in 9 columns, has been followed for about 100 ps. In view of the long time scale that characterizes the dynamics of these systems, significantly longer simulations, like those currently feasible, are necessary to make sure that the choice of the initial configuration does not affect the calculated properties. In addition, we point out that an MD simulation with an all-atom potential has been recently carried out[33] on a isolated column consisting of 4 HAT6 molecules;

† Scuola Normale Superiore.
‡ Universita di Pisa.
§ E-mail: g.cinacchi@sns.it.
|| Universita di Bologna.
⊥ E-mail: r.colle@sns.it.
# E-mail: tani@dcci.unipi.it.

10.1021/jp049654a CCC: $27.50 
Published on Web 05/15/2004

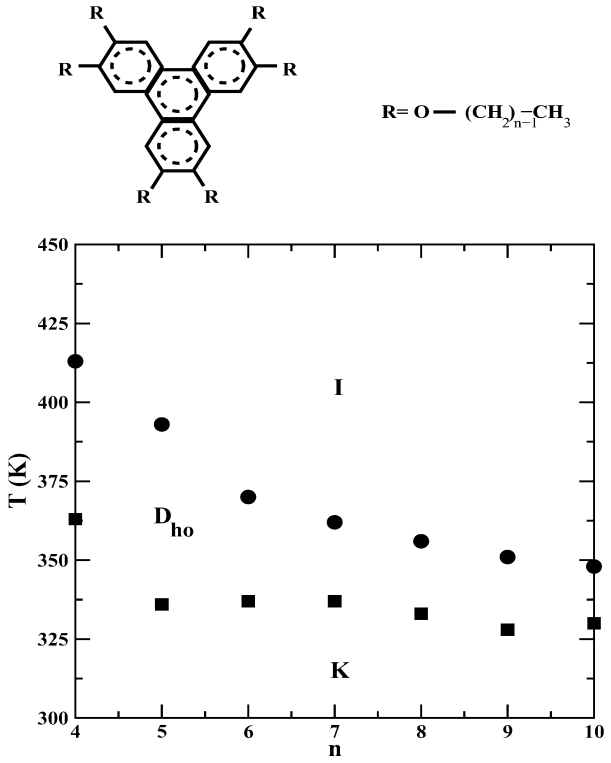


**Figure 1.** Chemical structure and experimental phase diagram of the HATn series: K = crystalline phase; $D_{ho}$ = hexagonal ordered columnar phase; I = isotropic phase. The phase transition temperatures, identified by dots and squares, have been taken from Figure 3 of ref 30.

this simulation has been combined with quasi-elastic neutron experiments performed on the columnar and isotropic phase of HAT6 to study molecular motions occurring on a 1−10 ps time scale.

The columnar state of HAT5 is also the subject of the present paper. Though the structure of the $D_{ho}$ phase appears rather clear from X-ray diffraction experiments, no definite answers on the conformational equilibria of the chains have been provided by the analysis of NMR data. In our atomistic MD simulations, we have calculated bulk and molecular structure of a columnar system of HAT5 model molecules, comparing our results with experimental data. The quality of the results can be considered a test of the atomistic model adopted, where well assessed experimental data are available for comparison, but our simulations give also additional information, not easily accessible from experiments, especially on the translational dynamics along directions parallel and perpendicular to the column axis.

The paper is organized as follows: section II contains a description of the model and its parameters; section III provides computational details on the molecular dynamics simulations, whose results are presented and discussed in section IV; conclusions are drawn in section V.

## 2. Model Potential

The HAT5 molecule consists of a triphenylene core linked with six pentyloxy chains. In Figure 2 the chemical structure of the HAT5 model molecule used in the computer simulations is shown. We notice that only the hydrogen atoms belonging to the aromatic rings of the central core are explicitly considered, whereas the united atom approach has been adopted for the alkyl chains. Eight different types of atoms are defined in the model: aromatic carbons of the central ring ($C_B$), aromatic carbons of the outer rings bonded to the aromatic hydrogens ($C_{BH}$), aromatic carbons bonded to the oxygens ($C_{BO}$), hydrogens (H), oxygens

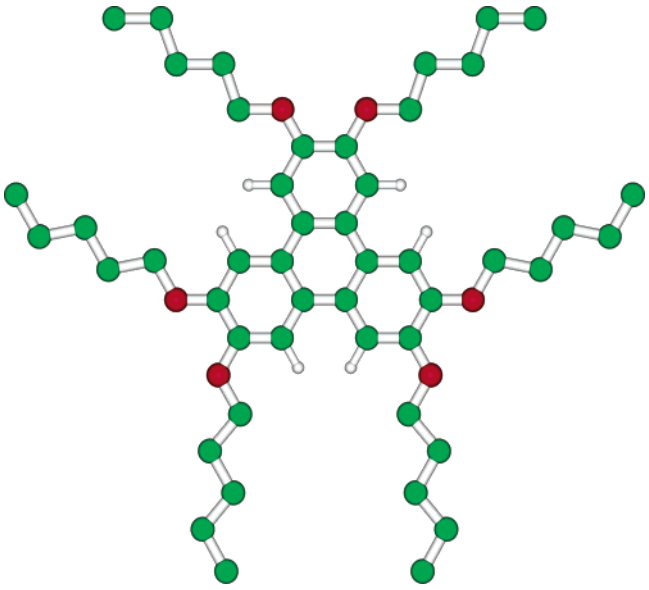

**Figure 2.** Model molecule HAT5 used in the MD simulations. Notice that the methylene and methyl groups of the aliphatic chains have been considered as a single interaction site, according to the united atom approach.

**TABLE 1: Equilibrium Bond Distances**[a]

| bond | $r_0$ (Å) |
|---|---|
| $C_{B(H,O)}-C_{B(H,O)}$ | 1.40 |
| $C_{BH}-H$ | 1.08 |
| $C_{BO}-O$ | 1.36 |
| $O-C_O$ | 1.43 |
| $C_{(O,2)}-C_{(2,3)}$ | 1.53 |

[a] Parentheses mean that no differences have been made between the included types of atoms.

(O), first aliphatic carbon of each chain ($C_O$), aliphatic carbons representing either a methylene group ($C_2$) or a terminal methyl group ($C_3$).

The potential energy of the system is given by the following sum of contributions:

$$E = \sum_{\text{angles}} \frac{1}{2} K_\vartheta (\vartheta - \vartheta_0)^2 + \sum_{\text{dihedrals}} \left[ \frac{V_1}{2}(1 + \cos\varphi) + \frac{V_2}{2}(1 - \cos 2\varphi) + \frac{V_3}{2}(1 + \cos 3\varphi) \right] + \sum_i \sum_{j>i} \left\{ \frac{q_i q_j}{r_{ij}} + 4\epsilon_{ij} \left[ \left( \frac{\sigma_{ij}}{r_{ij}} \right)^{12} - \left( \frac{\sigma_{ij}}{r_{ij}} \right)^{6} \right] \right\} \quad (1)$$

The first two terms correspond to the energy, $E_b$, due to bonded interactions, i.e., those intramolecular forces that depend on the chemical connectivity of the atoms; $E_b$ is decomposed into a sum of bond-bending (1−3 interactions) energies, each one represented by a harmonic potential ($\vartheta_0$ is the equilibrium angle), and a sum of torsional (1−4 interactions) energies, each one a function of a dihedral angle $\varphi$. In our simulations we have constrained all the bond distances to their equilibrium values, $r_0$, thus disregarding the bond-stretching (1−2 interactions) contribution to $E_b$. The parameters of the bonded interactions are listed in Tables 1−3.

The last double sum in eq 1 corresponds to the energy, $E_{nb}$, due to nonbonded interactions, i.e., those depending on the distance between two interacting atoms. $E_{nb}$ is given by the Coulomb and Lennard-Jones terms, with $q_i$, $q_j$ the effective point

**TABLE 2: Force Constants and Equilibrium Angles[a]**

| angle | $K_\vartheta$ (kJ·mol$^{-1}$·rad$^{-2}$) | $\vartheta_0$ (deg) |
|---|---|---|
| $C_{B(H,O)}-C_{B(H,O)}-C_{B(H,O)}$ | 527.2 | 120.00 |
| $C_{B(O)}-C_{BH}-H$ | 292.9 | 120.00 |
| $C_{BH}-C_{BO}-O$ | 527.2 | 120.00 |
| $C_{BO}-O-C_O$ | 527.2 | 120.00 |
| $O-C_O-C_2$ | 502.1 | 109.47 |
| $C_{(O,2)}-C_2-C_{(2,3)}$ | 502.1 | 109.47 |

[a] Parentheses mean that no differences have been made between the included types of atoms (see AMBER force field[42]).

**TABLE 3: Parameters of the Torsional Potentials[a]**

| dihedral | $V_1$ (kJ·mol$^{-1}$) | $V_2$ (kJ·mol$^{-1}$) | $V_3$ (kJ·mol$^{-1}$) |
|---|---|---|---|
| $X-C_{B(H,O)}-C_{B(H,O)}-X$ | 0.00 | 121.34 | 0.00 |
| $C_{BH}-C_{BO}-O-C_O$ | 0.00 | 9.20 | 0.00 |
| $C_{BO}-O-C_O-C_2$ | 8.94 | −4.44 | 11.78 |
| $C_{(O,2)}-C_2-C_2-C_{(2,3)}$ | 5.90 | −1.14 | 13.16 |

[a] X can be an aromatic carbon or a hydrogen or a oxygen. Parentheses mean that no differences have been made between the included types of atoms (see AMBER[42] and OPLS[43−45] force fields).

**TABLE 4: Parameters for Nonbonded Interactions Taken from the OPLS Force Field[43−45]**

| atom | $q$ (e) | $\epsilon$ (kJ·mol$^{-1}$) | $\sigma$ (Å) |
|---|---|---|---|
| $C_B$ | 0.0 | 0.293 | 3.550 |
| $C_{BH}$ | −0.115 | 0.293 | 3.550 |
| $C_{BO}$ | 0.135 | 0.293 | 3.550 |
| H | 0.115 | 0.125 | 2.420 |
| O | −0.385 | 0.711 | 3.000 |
| $C_O$ | 0.250 | 0.494 | 3.800 |
| $C_2$ | 0.0 | 0.494 | 3.905 |
| $C_3$ | 0.0 | 0.732 | 3.905 |

charges on the sites $i$, $j$ separated by a distance $r_{ij}$, and $\epsilon_{ij}$ and $\sigma_{ij}$ the well depth and contact distance of the two sites. The interaction potential between two atoms of the same type has its own set of parameters $\{q, \epsilon, \sigma\}$, whereas that between two different atoms is given in terms of parameters that are the geometrical mean of those for the two pairs of identical atoms. Note that 1−2, 1−3 and also 1−4 interactions do not contribute to the above double sum; furthermore, interactions between pairs of sites belonging to the central aromatic core have been excluded. The parameters of the nonbonded interactions are given in Table 4.

As a first test of the chosen empirical potential, we have calculated the interaction energy of two HAT5 molecules as a function of the distance (r) between two centers of mass, of the reciprocal rotation angle ($\alpha$) around the main axis ($\alpha = 0$ corresponds to cores superimposed), and of the chain conformation with respect to the plane of the core. Figure 3 shows the contour plot in the $(r, \alpha)$ plane of the dimer interaction energy for the face-to-face configuration with the equatorial chains in all-trans conformations and the dihedral angles $C_B-C_{BO}-O-C_O$ set at 180°, as in Figure 2. This conformation is often called *diablo-like* and is that of minimum energy, according to recent semiempirical calculations.[46] The energy minimum we found for this configuration is −209.1 kJ·mol$^{-1}$, at $r = 3.8$ Å and $\alpha = 60°$. Conversely, that of an *octopus-like* configuration, with the $C_B-C_{BO}-O-C_O$ dihedral angles equal to ±90° and chains alternatively above and below the triphenylene plane, is $E_{min} = -175.0$ kJ·mol$^{-1}$ at $r = 3.8$ Å with $\alpha$ equal to 20°.

## 3. Molecular Dynamics Simulations: Computational Details

We have considered a system of $N = 80$ HAT5 molecules, corresponding to a total of 4800 interacting sites. The system has been held at a pressure P = 0.1 MPa and a temperature T = 375 K by Berendsen's method,[47] with pressure and temperature relaxation times of 2 and 1 ps, respectively. The simulation cell was a parallelepiped of edges $L_x$, $L_y$, and $L_z$, with periodic boundary conditions. The equations of motion have been integrated with a time step of 2 fs,[48] using Verlet's algorithm in the leapfrog version.[49] All the bond lengths have been constrained at their equilibrium value (see Table 1) by the SHAKE method.[50] The intermolecular Lennard-Jones interactions have been truncated at $r_{cut} = 10$ Å, and the long-range corrections to energy and virial included in the standard way.[51] The computation has been speeded up by employing the neighbor-list-linked-cell method[49] with radius of 12 Å and automatic updating. The electrostatic interactions have been summed using the Ewald method[52] with a convergence parameter of 0.2685 Å$^{-1}$. The set of reciprocal lattice vectors, $\mathbf{k} = 2\pi(n_x/L_x, n_y/L_y, n_z/L_z)$, $n_x = 1-20$, $n_y = 1-12$, $n_z = 1-10$, has been chosen with a cutoff $k_{cut}^2 = 4\pi^2 n_{cut}^2/\min\{L_x^2, L_y^2, L_z^2\}$, and $n_{cut}^2 = 50$. The initial configuration was an hexagonal arrangement of columns, each consisting of 10 molecules, whose conformation was that of Figure 2. Nearest neighbor molecules in each column have been mutually rotated by 60° around their principal axis. The distance among the columns in the starting configuration has been slightly increased to avoid site superposition. The system has been equilibrated for 8.5 ns to ensure that no long-time drifts were present in the monitored properties. Then, a 2 ns production run has been performed to store configurations necessary for the time averaging of the quantities of interest. A further 1 ns run has been carried out in the microcanonical ensemble to calculate dynamical properties. Finally, an 1 ns MD run has been performed on an isolated molecule with an internal energy corresponding to $T = 375$ K, starting from the conformation given in Figure 2. All the calculations have been executed with the parallel version of the freely available MOSCITO program.[53] Typically, each MD step took about 0.5 s on a cluster of 4 PCs (each one equipped with an Intel Xeon 2.80 GHz processor) running under Linux OS.

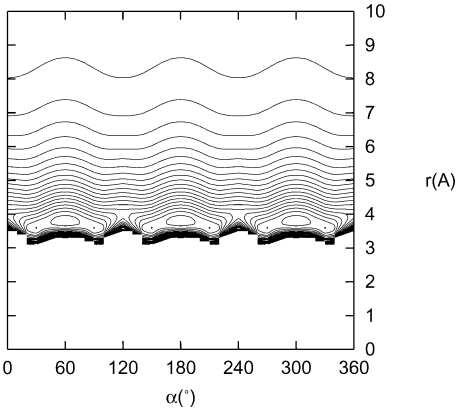


**Figure 3.** Contour plot of the dimer interaction energy for the face-to-face configuration, as a function of the distance of the centers of mass and of the rotation angle around the $C_3$ axis of the core. For both the interacting molecules, the conformation of the chains is all-trans and they lie in the plane of the core: *diablo-like* conformation. Curves are plotted from −200 to 0 kJ·mol$^{-1}$ in steps of 10.

## 4. Results and Discussion

**4.1. Thermodynamic Properties.** We begin the discussion of our results by presenting in Table 5 the energy values obtained for a system of an average density $\rho = 1.003$ g/cm$^3$, about 6% lower than that typical of an experimental sample.[23]

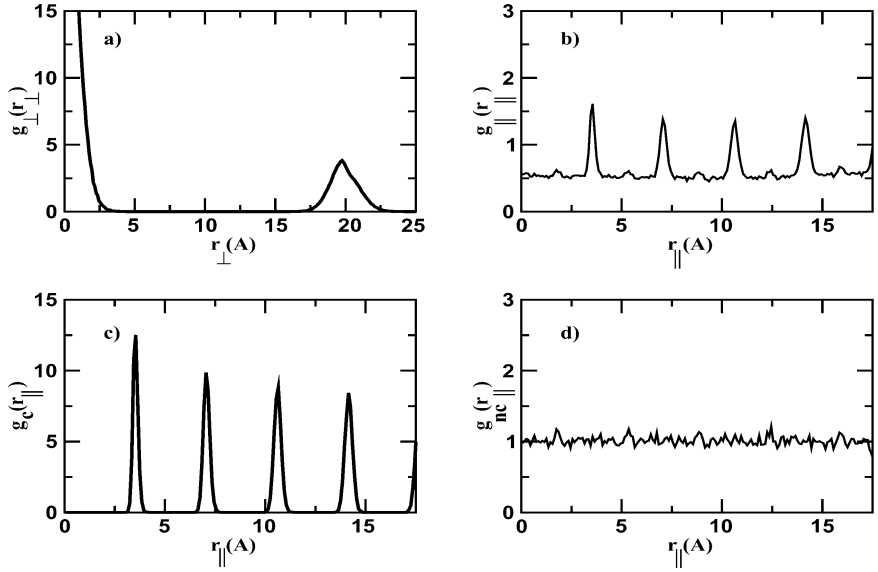


**Figure 4.** Positional correlation functions: (a) perpendicular; (b) parallel; (c) columnar, (d) nearest column.

**TABLE 5: Intramolecular Energy, $E_{intra}$, and Interaction Energy, $E_{inter}$, Decomposed into Their Contributions for an Isolated and a Bulk Molecule[a]**

| | $E_{intra}$ | $E_{ben}$ | $E_{tor}$ | $E_{nb}$ | $E_{inter}$ | $E_{LJ}$ | $E_{qq}$ |
|---|---|---|---|---|---|---|---|
| isolated | 29.0 | 93.0 | 167.0 | −231.0 | 0.0 | 0.0 | 0.0 |
| bulk | 17.0 | 93.0 | 136.0 | −212.0 | −285.0 | −275.0 | −10.0 |

[a] All energies are in kJ·mol$^{-1}$.

We notice that passing from the isolated molecule to the condensed phase system, the intramolecular energy reduces, because the less negative contribution from nonbonded interactions is compensated by a larger gain in torsional energy. This fact shows the importance of environmental effects that are able to force the dihedral angles closer to the value corresponding to the energy minimum, a trans state, than in the case of an isolated molecule. Furthermore, we observe that the van der Waals contribution to the intermolecular energy is dominant, about 96.5% of the total vs just 3.5% from the electrostatic interactions.

**4.2. Orientational and Positional Order.** A key quantity in the study of liquid crystals is the orientational order parameter ($\eta$), which we have calculated by considering only the aromatic triphenylene core of each HAT5 molecule. The plane of the core can be defined by two vectors joining its center of mass with two oxygen atoms on the nearby outer phenyl rings. The following **Q** tensor,[54]

$$Q_{\alpha\beta} = \frac{1}{2N}\sum_{i=1}^{N}(3u_{i\alpha}u_{i\beta} - \delta_{\alpha\beta}) \qquad \alpha, \beta = x, y, z \qquad (2)$$

is built in terms of unit vectors $\hat{\mathbf{u}}_i$ perpendicular to the core plane of the *i*th molecule. Note that each vector is defined in the laboratory frame, with the columns that, at the beginning of the simulation, are oriented in the direction of the *z* axis. The largest eigenvalue of **Q** is defined as the instantaneous order parameter and the corresponding eigenvector taken as the director ($\hat{\mathbf{n}}$) of the system. The time averaging gives $\eta = 0.984$, a value slightly higher than those measured in real experiments,[24,26] which range from 0.85 to 0.95.

To characterize the bulk structure of the liquid crystal, we have calculated four positional correlation functions, shown in Figure 4:

(a) The perpendicular correlation function, $g_\perp(r_\perp)$, that gives information on the arrangement of molecules in planes perpendicular to the director and represents the conditional probability of finding the center of mass of another molecule at a distance r from the reference molecule, such that $r_\perp = |\mathbf{r} \times \hat{\mathbf{n}}|$.

(b) The parallel correlation function, $g_{||}(r_{||})$, that gives the conditional probability of finding the center of mass of another molecule at a distance *r* from the reference molecule, such that $r_{||} = \mathbf{r}\cdot\hat{\mathbf{n}}$.

(c) The columnar correlation function, $g_c(r_{||})$, that gives the conditional probability of finding another molecule of the same column at a distance $r_{||}$ along the director.

(d) The nearest column correlation function, $g_{nc}(r_{||})$, that gives the conditional probability of finding the center of mass of another molecule of a nearest neighbor column at a distance $r_{||}$ along the director.

The perpendicular correlation function, shown in Figure 4a, is characterized by a large peak around 0, which is due to molecules in the same column. The other peak, centered around $r_\perp = 19.75$ Å, has a width ∼5 Å and is partly due to in plane nearest neighbors; this value of $r_\perp$ is consistent with the intermolecular in plane distance of 18.95 Å, estimated from X-ray diffraction experiments.[23] Both the measured and calculated values are smaller than the diameter of the molecule in the fully stretched conformation (see Figure 2). Because of its broad structure, the in plane nearest neighbor peak does not allow by itself identification of a specific two-dimensional lattice. We have therefore calculated the following bond orientational order parameter:[55]

$$\Psi_6 = \left\langle \frac{\left|\sum_{i=1}^{N-1}\sum_{j>i}^{N} p_{ij}\exp(\mathrm{i}6\vartheta_{ij})\right|}{\sum_{i=1}^{N-1}\sum_{j>1}^{N} p_{ij}} \right\rangle$$

$$p_{ij} = \begin{cases} 1 & 17.5 \le r_{\perp ij} \le 22.5 \\ 0 & \text{otherwise} \end{cases} \qquad (3)$$

where $\vartheta_{ij}$ is the angle between the intermolecular vector $\mathbf{r}_{ij}$ that joins the centers of mass of two molecules and a given axis in the plane orthogonal to the director. Note that $\Psi_6 = 1$ in the case of perfect hexagonal order whereas $\Psi_6 = 0$ indicates the

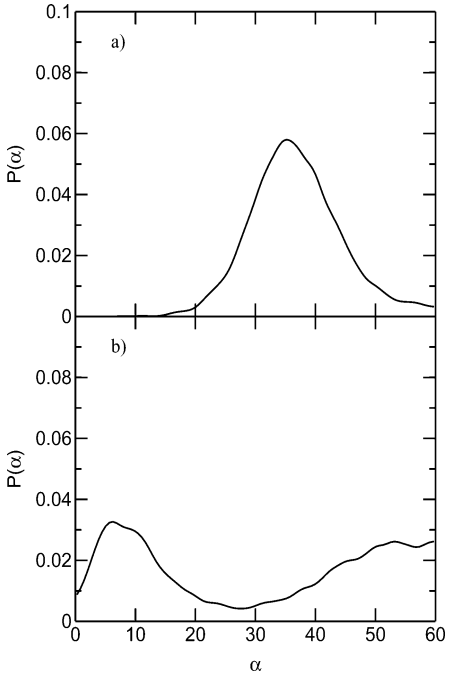


**Figure 5.** Distribution function $P(\alpha)$ for (a) nearest neighbor molecules in a column and (b) second nearest neighbor molecules in a column.

complete lack of such order. Our simulation gives $\Psi_6 = 0.87$, a value suggesting that the initial hexagonal organization of the columns is substantially maintained during the simulation. The parallel correlation function, shown in Figure 4b, is characterized by a series of narrow peaks, equally spaced by 3.55 Å, a value almost coincident with that of 3.6 deduced from experiments.[23] If we consider that two HAT5 molecules in the face-to-face configuration have a minimum energy distance of 3.8 Å (see section II), we see that the columnar environment has a significant effect. The peaks of the parallel correlation function indicate an ordered stacking of the molecules within a column, which is confirmed also by the columnar correlation function shown in Figure 4c. Finally, we observe that the parallel correlation function is almost constant between two contiguous peaks, which suggests a lack of positional correlation among molecules belonging to different columns, as also proved by the featureless nearest column correlation function of Figure 4d.

In the above analysis of the bulk structure via order parameters and correlation functions of the center of mass distances, we have implicitly assumed a uniaxial approximation of the molecular cores, which are actually characterized by $D_{3h}$ symmetry. Hence, it is of interest to investigate how such "equilater triangles" pile up in a column. To get this information, we have calculated the distribution function, $P(\alpha)$, of the angle defined in section II, for nearest neighbor and second nearest neighbor molecules in the same column. The two distributions are shown in Figure 5a,b, respectively, for $0° \le \alpha \le 60°$, where $\alpha = 0°$ corresponds to superimposed triphenylene cores and $\alpha = 60°$ to a star configuration of the two triangles. We see that the nearest neighbor distribution (Figure 5a) peaks around $\alpha^* = 36°$ and the second neighbor distribution (Figure 5b) is characterized by a peak at $\sim 8°$ and a broad band at $\sim 55°$. Because two nearest neighbors in the same column are rotated with respect to each other by an angle, on average, $\alpha^*$, there are two possibilities of mutual rotation for columnar second nearest neighbors. The first one corresponds to a backward rotation of $\alpha^*$, leading to almost overlapping second nearest neighbors (ABA stacking); the second is a forward rotation of $\alpha^*$, leading to second nearest neighbors rotated by an angle of $2\alpha^*$ (ABC stacking). From Figure 5 we conclude that in our simulated system there is an equal probability of both stackings. This is consistent with the possibility that the molecules in a column may have a helicoidal arrangement, also suggested by the analysis of experimental data.[23] If we assume $\alpha^* = 36°$, we obtain a helical pitch of 12 Å, which compares fairly well with its experimental counterpart of 13 Å.

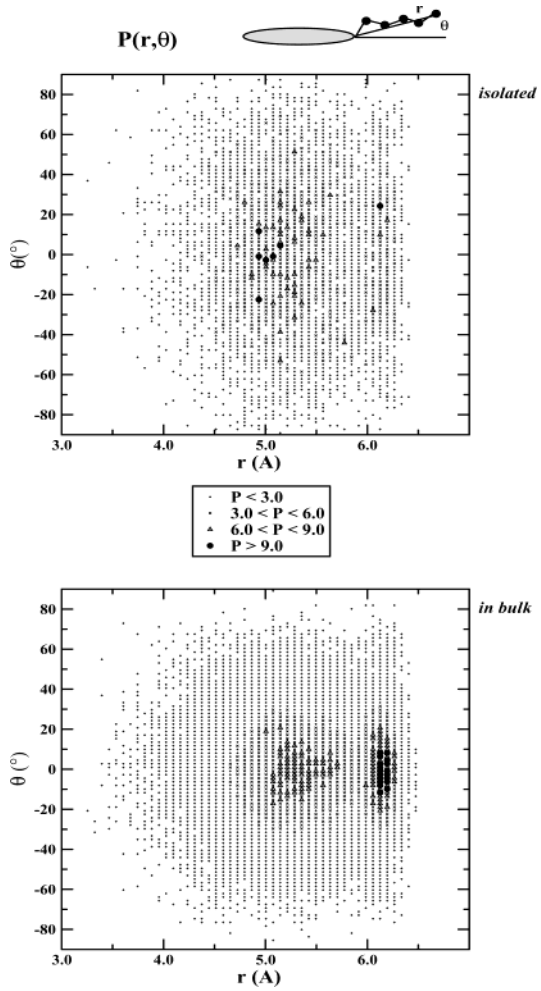


**Figure 6.** Distribution function $P(r,\theta)$ of the chain length orientation with respect to the plane of the core, for an isolated and a bulk molecule.

**4.3. Molecular Structure.** In this section, we present results concerning the average length and orientation of the pendant chains and their internal degree of order. We have calculated the distribution function, $P(r,\theta)$, of the chain length, $r$, defined as the length of the vector joining the terminal methyl group and the oxygen atom, and of the angle, $\theta$, that such a vector forms with the triphenylene plane. The results are shown in Figure 6 for both an isolated and a bulk molecule in the columnar condensed structure. We see that, though the isolated molecule has a broad distribution with maxima around $r \sim 5$ Å and $\theta \sim 0°$, a bulk molecule in the columnar state is characterized by a distribution function with two maxima both around $\theta = 0°$: the absolute one is located around r $\sim$ 6.2 Å, and the other one is around $r \sim 5.4$ Å. The chain conformation corresponding to the first maximum is a stretched, all-trans one, whereas the presence of another maximum at shorter distances suggests a significant population of gauche states for at least some of the dihedral angles. The chains have the highest probability to lie in the plane of the core ($\theta = 0°$) but excursions up to 30° above or beneath such a plane are not rare.

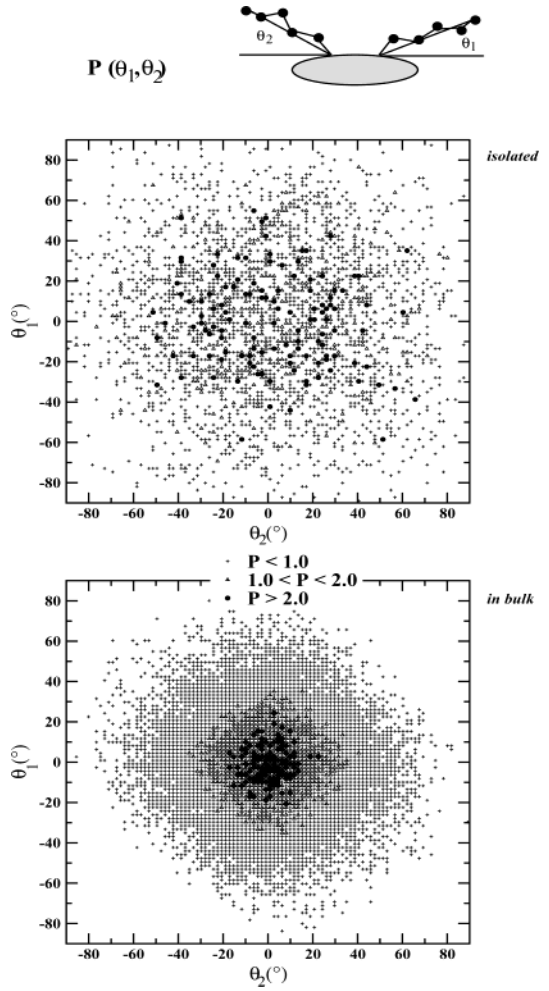


**Figure 7.** Distribution function $P(\theta_1,\theta_2)$ of the angle made by two adjacent chains with the plane of the core, for an isolated and bulk molecule.

We have also calculated the distribution function, $P(\theta_1,\theta_2)$, of the angles that two chains, bonded to the same outer phenyl ring, form with the plane of the core. This function is plotted in Figure 7, both for an isolated and a bulk molecule.

It is worth noting the high symmetry of both distributions (as well as of that plotted in Figure 6) with respect to reflections through the molecular plane, a feature that confirms the good statistical accuracy of the simulation. We observe a large difference between the two distributions. It is apparent that the relevant angles are much more evenly distributed for an isolated molecule. The distribution of a molecule in the bulk phase (Figure 7, lower panel) has a maximum at (0°;0°) and an overall shape resembling a square, with diagonals parallel to the axes and significant density up to (±30°;0°) and (0°;±30°). This suggests that when a chain is above or below the aromatic plane, the nearest one tends to remain on such a plane.

Experimental data do not lead to a single and consistent picture of chain length and orientation. $^{13}$C NMR experiments[26] indicate, indeed, that the chains should lie on the plane of the core with *diablo-like* conformation, whereas, $^{2}$H NMR experiments[27] were interpreted as consistent with *octopus-like* arrangement. Our numerical experiments do not completely support either of these two extreme pictures, rather they suggest a somewhat intermediate situation. On one hand, it is clear that the chains prefer to lay stretched on the plane of the core, and there is no indication that, when a chain is above the plane, the contiguous one should necessarily stay below it. On the other hand, configurations characterized by a smaller extension ($r$) and significant values of the angle ($\theta$) above or below the plane of the core have non negligible probability.

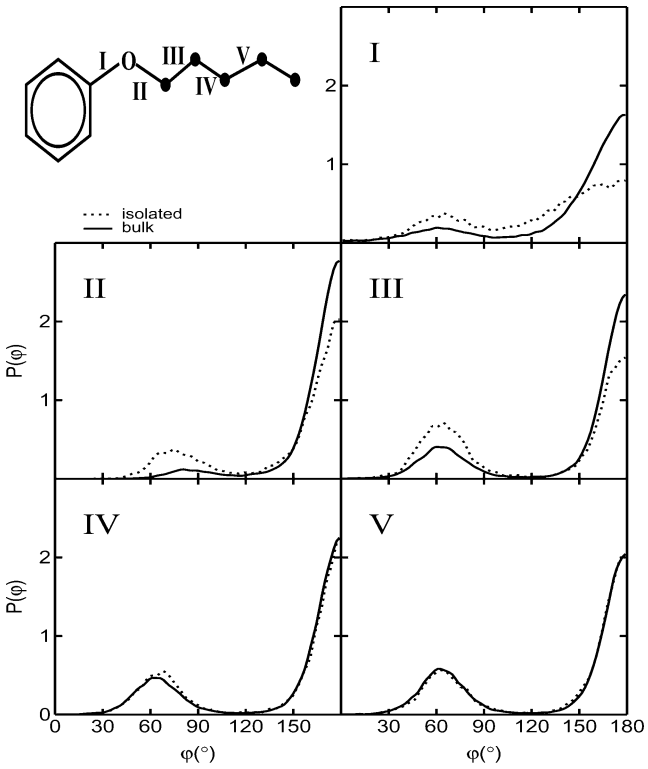


**Figure 8.** Distribution function of the dihedral angles around the bonds indicated on the top left.

The conformation of the alkyl chains have also been analyzed through distribution functions, $P(\varphi)$, of the five dihedral angles shown in Figure 8. The distribution function of the dihedral angle I is fairly broad, with a large difference between isolated and columnar phase, in the latter becoming more structured; the angular region around 60°, corresponding to the gauche states has a rather flat probability distribution whereas the band corresponding to the trans state, which turns out to be the most probable in both phases, has a shape consistent with the already discussed tendency of the chains to make some excursions above and below the plane of the core, making angles less than ∼30° (see Figures 6 and 7). On the contrary, the dihedral angle II is quite stiff, with a high probability for the trans conformation, especially in the bulk phase. The second peak of the distribution $P_{II}(\varphi)$ is located at a value larger than 60° also in the isolated molecule; in the bulk, its amplitude is very reduced and its location is displaced at 80°. The distribution function of the dihedral angles III, IV, and V presents two well-resolved peaks, the higher one corresponding to the trans state and the other to the gauche state. We notice that the difference between distribution functions for isolated and bulk molecules reduces along the chain, until it vanishes for the dihedral angle V, an indication that the chains tend to become more and more disordered as the distance from the core increases. Finally, if we focus on the value of the distribution function of an isolated molecule at 180°, we observe an alternating behavior from I to V, with the difference between two successive values decreasing when moving away from the core: a sort of odd−even effect that is missing in the columnar state.

A deeper insight into the arrangement of the side chains can be gained by calculating the distribution function of the conformers, both in the columnar and in the gas phase. The frequency of occurrence of the $2^5$ states is shown in Table 6;

**TABLE 6: Population of the Conformations of the Pendant Chains[a]**

| conformation | isolated (%) | columnar (%) |
|---|---|---|
| *gtggt* | 3.42 | 0.87 |
| *gtgtg* | 4.77 | 2.28 |
| *gtgtt* | 5.63 | 2.84 |
| *gttgt* | 5.27 | 3.13 |
| *gtttg* | 4.28 | 3.98 |
| *gtttt* | 4.95 | 4.55 |
| *tgtgt* | 3.40 | 2.60 |
| *tgttg* | 3.77 | 0.75 |
| *tgttt* | 3.68 | 1.38 |
| *ttggt* | 5.67 | 2.22 |
| *ttgtg* | 7.50 | 7.73 |
| *ttgtt* | 10.88 | 8.77 |
| *tttgt* | 6.95 | 15.50 |
| *ttttg* | 5.47 | 16.33 |
| *ttttt* | 6.38 | 19.90 |

[a] *g* indicates both gauche states; *t* indicates the trans state. Only conformers with a frequency larger than 3% are reported.

for the sake of brevity, only those states with a population larger than 3% in both phases are reported.

The data of Table 6 confirm that the main difference between the isolated and bulk molecule is an increase of the population of the most stretched conformers, to the expense of those conformations with a gauche state for the first dihedral angle. Comparison of these results with the experimental data of ref 27 is hampered by a lack of data for many conformers, neglected in their analysis, and by the undefined value of the probability of the conformer *gtgtt*, referred to as $P_4$ in Table 4 of the same paper. Assuming for $P_4$ the value we calculated (2.84%), which is close to the lower limit of the range allowed to this parameter ($0 \leq P_4 \leq 31.4\%$; see Table 4 of ref 27), we obtain the following percentage populations: 21.9 (*gtttt*), 23.0 (*ttgtt*), 16.9 (*tttgt*), 35.6 (*ttttt*).

It must be stressed that the (at best) fair agreement between calculated and experimental frequencies is strongly dependent on the assumptions made in the experimental data treatment, so that the comparison we can make is much less straightforward than would be necessary for an accurate test of the simulation results.

The comparison with experimental data becomes less cumbersome if one considers the behavior of the orientational order parameter of the C−H bonds in the alkyl chains, $S_{CH}$, as a function of the bond position in the chain. The order parameters of the methylene groups, calculated by exploiting the method described in ref 56, are compared with those obtained in ref 27 by $^2$H NMR experiments in Figure 9.

We see that the overall experimental trend is correctly reproduced by the simulation, although the calculated values overestimate the experimental ones. The $S_{CH}$ order parameter decreases on moving from the methylene group labeled $C_O$ to the last methylene group linked to the terminal methyl, a further indication that the chain motion becomes less hindered moving away from the core. Analogous conclusions have been drawn also in ref 26 by anayzing the data from $^{13}$C NMR experiments.

To conclude this section, we can say that, although the aromatic cores are characterized by a high degree of two-dimensional positional and orientational order, the alkyl chains of the HAT5 molecule in the columnar phase are in a liquidlike state.

**4.4. Translational Dynamics.** The structural properties so far discussed indicate that the simulated system of HAT5 molecules shows a bulk and molecular structure in reasonable agreement with the experimentally deduced picture of a $D_{ho}$ phase of real HAT5. In this section, we demonstrate that the system we are studying is not amorphous but has a liquid-crystal-like dynamics. To this end, we have calculated the mean square displacement (MSD) of the molecular center of mass along the *x*, *y*, and *z* axes of the laboratory frame. The MSD is defined as follows:

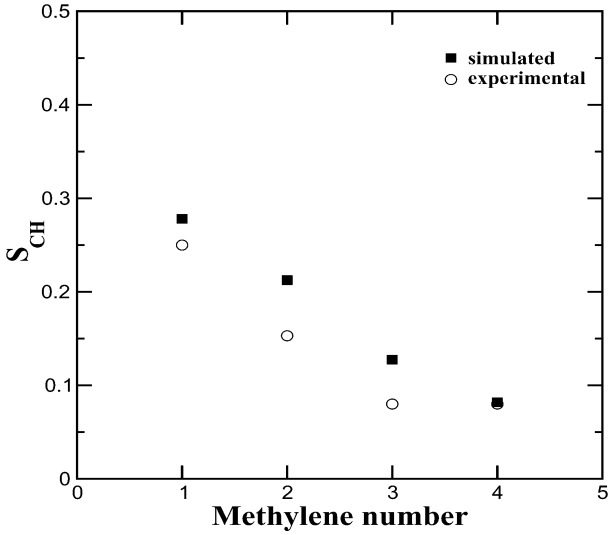


**Figure 9.** $S_{CH}$ order parameter of the various methylene groups ($S_{CD}$ in the experiments).

$$\mathrm{MSD(t)} = \langle [r(t) - r(0)]^2 \rangle \tag{4}$$

where the average is taken over all molecules and the configurations generated in the microcanonical (NVE) ensemble. In an anisotropic system like that we are studying, it is natural to resolve MSD in a reference frame defined by the director and two axes transverse to it.

Our results, plotted in Figure 10a, show that the MSD along *x* and *y* is characteristic of a solid-state system, converging, eventually, to constant values. The small difference between the two transverse directions is only visible on a "short" time scale, as the motion along *y* is less constrained up to ∼150 ps. This can be understood by looking at Figure 11a, which shows the *x* and *y* coordinates of the center of mass of each molecule in the first and in the last configuration of the microcanonical run. A two-dimensional hexagonal arrangement of particles is equivalent to a centered-rectangular arrangement of edges $a = d\sqrt{3}$ and $a_y = d$, where *d* is the diameter of the particles. It follows that the movement of a particle is less constrained along *y* than along *x*. The solidlike behavior we observe, perpendicularly to the director, is in substancial agreement with recent NMR experiments[32] that yield a diffusion coefficient, $D_\perp$, of order $10^{-14}$ m$^2$/s. In the same work,[32] no data are reported for the diffusion coefficient along the director, that, however, according to the authors, should be even smaller, because of the shape anisotropy that should favor diffusion normal to the director in a discotic mesophase. Figure 10a, however, apparently shows a significant motion along the director ($\hat{\mathbf{z}}$). This picture might be misleading, if taken at face value, for a system like HAT5, which certainly is no ordinary liquid. In this case, it is necessary to extract from the motion of every molecule a "collective" part, related to the dynamics of the center of mass of each column, plus a contribution given by the relative motion of the molecular center of mass with respect to the center of mass of its column. The results of this analysis are shown in Figure 10b. It turns out that almost the whole "diffusive" dynamics is actually due to the motion of the column as a whole,

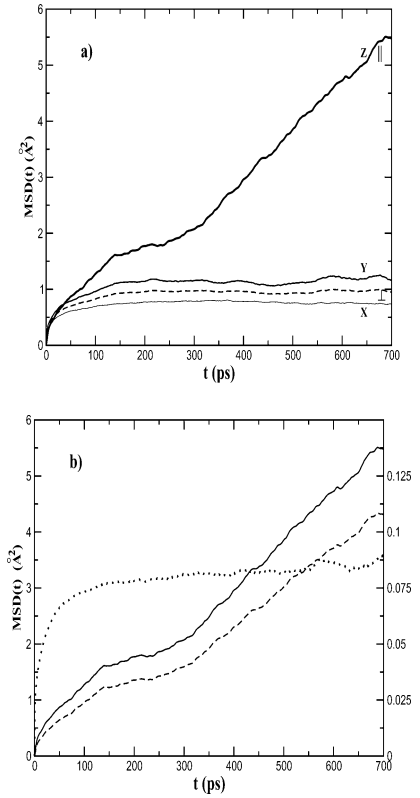


**Figure 10.** (a) Mean square displacement (MSD) of the molecular center of mass along *x*, *y* and *z* (which is parallel to the director). The dashed curve labeled ⊥ is the average of the *x* and *y* curves. (b) Total molecular MSD (solid), MSD of the column center of mass (dashed) and relative molecular MSD (dotted) along the director. Notice that the vertical axis of the dotted curve is that on the right.

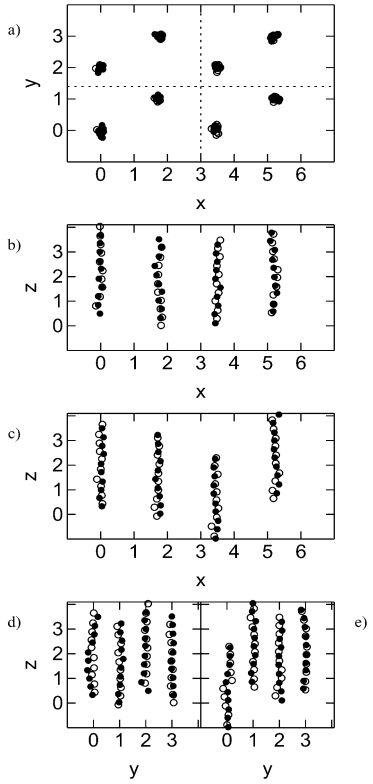


**Figure 11.** Center of mass coordinates of the molecules in the initial (white) and final (black) configuration of the microcanonical run: (a) projection in the *xy* plane; (b) projection in the *xz* plane of the four columns above the horizontal dotted line of (a); (c) same as (b), for the columns below the horizontal dotted line of (a); (d) projection in the *yz* plane of the four columns left of the vertical dotted line of (a); (e) same as (d) for the columns right of the vertical dotted line of (a). Note that the units of length are nanometers.

whereas the relative diffusion leads to a MSD $\approx 0.1$ Å$^2$ after 1 ns, about 2 orders of magnitude smaller than that of the columnar motion. One should also observe that the latter dynamics might be artificially enhanced by the periodic boundary conditions, which render these structures quasi-infinite, in a small system free of defects. Hence, these results should be considered as a sort of upper limit to the diffusion coefficient, whereas a more sensible comparison with experimental data should involve the results of the MSD that correspond to the relative molecular motion (see dotted line in Figure 10b).

As a matter of fact, the liquidlike behavior of the MSD along the director, should be traced back to the mutual sliding motion of the columns. Figure 11b−e shows the 8 columns of the initial and final configurations of the NVE run from different perspectives. We see that the columns have moved alternatively up and down. Furthermore, they are not perfectly linear but present slight distortions with a somewhat helicoidal shape.

## 5. Conclusions

The results so far obtained from our MD simulation based on the OPLS force field indicate that the description of the columnar phase of HAT5 at $T = 375$ K and ambient pressure is fairly close to that provided by the experimental data.

From the structural point of view, the model overestimates the orientational order parameter and the column-to-column distance but does not contradict the possibility of a helicoidal arrangement of the molecules in a column, with an estimated pitch (12 Å) within 10% of the experimental value, 13 Å.

The most probable chain configuration predicted by the simulation is that with fully stretched chains in the plane of the core, but the probability density of more compact conformations and nonzero angles is not negligible at all.

As already observed in other mesophases, the order parameter calculated for the methylene groups of the chains decreases as their distance from the core increases. This result is in agreement with the trend of the experimental data, although the calculation overestimates the measured values.

The dihedral angle distributions show that the columnar arrangement constrains these angles closer to their minimum energy values than in the case of an isolated molecule. This is consistent with the observed increase of the population of conformers with most dihedrals in the trans state when passing from the isolated to the columnar phase.

The translational diffusion coefficient (the only dynamical property calculated in this work) is solidlike for motions transverse to the column, in agreement with recent NMR measurements. The motion along the column axis appears much faster. This behavior is due to a coherent motion of groups of molecules belonging to the same column. Actually, the parallel diffusion coefficient would be even smaller than the transverse one, if calculated from the MSD of the *z* coordinate relative to the column center of mass.

**Acknowledgment.** Financial support of the Scuola Normale Superiore di Pisa is gratefully acknowledged.

## References and Notes

(1) Chandrasekhar, S.; Sadashiva, B. K.; Suresh, K. A. *Pramana* **1977**, *9*, 471.

(2) Billard, J.; Dubois, J. C.; Nguyen, H. T.; Zann, A. *Nouv. J. Chim.* **1978**, *2*, 535.
(3) Destrade, C.; Nguyen, H. T.; Gasparoux, H.; Malthete, J.; Levelut, A. M. *Mol. Cryst. Liq. Cryst.* **1981**, *71*, 111.
(4) Levelut, A. M. *J. Chim. Phys.* **1983**, *80*, 149.
(5) Chandrasekhar, S.; Ranganath, G. S. *Rep. Prog. Phys.* **1990**, *53*, 57.
(6) Chandrasekhar, S. *Liq. Cryst.* **1993**, *14*, 3.
(7) Boden, N.; Bushby, R. J.; Clements, J.; Jesudason, M. V.; Knowles, P. F.; Williams, G. *Chem. Phys. Lett.* **1988**, *152*, 94.
(8) Vaughan, G. B. M.; Heiney, P. A.; McCauley, J. P.; Smith, A. B., III. *Phys. Rev. B* **1992**, *46*, 2787.
(9) Boden, N.; Bushby, R. J.; Clements, J. *J. Chem. Phys.* **1993**, *98*, 5920.
(10) Adam, D.; Closs, F.; Frey, T.; Funhoff, D.; Haarer, D.; Schuhmacher, P.; Siemensmeyer, K. *Phys. Rev. Lett.***1993**, *70*, 457.
(11) Adam, D.; Haarer, D.; Closs, F.; Frey, T.; Funhoff, D.; Siemensmeyer, K.; Schuhmacher, P.; Ringsdorf, H. *Ber. Bunsen-Ges. Phys. Chem.* **1993**, *97*, 1366.
(12) Bengs, H.; Closs, F.; Frey, T.; Funhoff, D.; Ringsdorf, H.; Siemensmeyer, K. *Liq. Cryst.* **1993**, *15*, 565.
(13) Adam, D.; Schuhmacher, P.; Simmerer, J.; Haussling, L.; Siemensmeyer, K.; Etzbach, K. H.; Ringsdorf, H.; Haarer, D. *Nature* **1994**, *371*, 141.
(14) Boden, N.; Bushby, R. J.; Clements, J.; Movaghar, B.; Donovan, K. J.; Kreouzis, T. *Phys. Rev. B* **1995**, *52*, 13274.
(15) Arikainen, E. O.; Boden, N.; Bushby, R. J.; Clements, J.; Movaghar, B.; Wood, A. *J. Mater. Chem.* **1995**, *5*, 2161.
(16) Warman, J. M.; Schouten, P. G. *J. Phys. Chem.* **1995**, *99*, 17181.
(17) Boden, N.; Bushby, R. J.; Clements, J.; Donovan, K.; Movaghar, B.; Kreouzis, T. *Phys. Rev. B* **1998**, *58*, 3063.
(18) van der Craats, A. M.; Siebbeles, L. D. A.; Bleyl, I.; Haarer, D.; Berlin, Y. A.; Zharikov, A. A.; Warman, J. M. *J. Phys. Chem. B* **1998**, *102*, 9625.
(19) Chandrasekhar, S.; Prasad, S. K. *Contemp. Phys.* **1999**, *40*, 237.
(20) Boden, N.; Bushby, R. J.; Clements, J.; Movaghar, B. *J. Mater. Chem.* **1999**, *9*, 2081.
(21) Schmidt-Mende, L.; Fechtenkotter, A.; Mullen, K.; Moons, E.; Friend, R. H.; Mac Kenzie, J. D. *Science* **2001**, *293*, 1119.
(22) Pecchia, A.; Lozman, O. R.; Movaghar, B.; Boden, N.; Bushby, R. J.; Donovan, K. J.; Kreouzis, T. *Phys. Rev. B* **2002**, *65*, 104204.
(23) Levelut, A. M. *J. Phys. Lett.* **1979**, *40*, 81.
(24) Goldfarb, D.; Luz, Z.; Zimmermann, H. *J. Phys.* **1981**, *42*, 1303.
(25) Vilfan, M.; Lahajnar, G.; Rutar, V.; Blinc, R.; Topic, B.; Zann, A.; Dubois, J. C. *J. Chem. Phys.* **1981**, *75*, 5250.
(26) Rutar, V.; Blinc, R.; Vilfan, M.; Zann, A.; Dubois, J. C. *J. Phys.* **1982**, *43*, 761.
(27) Goldfarb, D.; Luz, Z.; Zimmermann, H. *J. Chem. Phys.* **1983**, *78*, 7065.
(28) Dong, R. Y.; Goldfarb, D.; Moseley, M. E.; Luz, Z.; Zimmermann, H. *J. Phys. Chem.* **1984**, *88*, 3148.
(29) Goldfarb, D.; Dong, R. Y.; Luz, Z.; Zimmermann, H. *Mol. Phys.* **1985**, *54*, 1185.
(30) Luz, Z.; Goldfarb, D.; Zimmermann, H. In *Nuclear Magnetic Resonance of Liquid Crystals*; Emsley, J. W., Ed.; Reidel: Dordrecht, The Netherlands, 1985; Chapter 14.
(31) Shen, X.; Dong, R. Y.; Boden, N.; Bushby, R. J.; Martin, P. S.; Wood, A. *J. Chem. Phys.* **1998**, *108*, 4324.
(32) Dvinskikh, S. V.; Furo, I.; Zimmermann, H.; Maliniak, A. *Phys. Rev. E* **2002**, *65*, 050702(R).
(33) Mulder, F. M.; Stride, J.; Picken, S. J.; Kouwer, P. H. J.; de Haas, M. P.; Siebbeles, L. D. A.; Kearley, G. J. *J. Am. Chem. Soc.* **2003**, *125*, 3860.
(34) Veerman, J. A. C.; Frenkel, D. *Phys. Rev. A* **1992**, *45*, 5633.
(35) Emerson, A. P. J.; Luckhurst, G. R.; Whatling, S. G. *Mol. Phys.* **1994**, *82*, 113.
(36) Bates, M. A.; Luckhurst, G. R. *J. Chem. Phys.* **1996**, *104*, 6696.
(37) Zewdie, H. *Phys. Rev. E* **1998**, *57*, 1793.
(38) Cinacchi, G.; Tani, A. *J. Chem. Phys.* **2002**, *117*, 11388.
(39) Caprion, D.; Bellier Castella, L.; Ryckaert, J. P. *Phys. Rev. E* **2003**, *67*, 041703.
(40) Maliniak, A. *J. Chem. Phys.* **1992**, *96*, 2306.
(41) Ono, I.; Kondo, S. *Bull. Chem. Soc. Jpn.* **1992**, *65*, 1057.
(42) Cornell, W. D.; Cieplak, P.; Bayly, C. I.; Gould, I. R.; Merz, K. M., Jr.; Ferguson, D. M.; Spellmeyer, D. C.; Fox, T.; Caldwell, J. W.; Kollman, P. A. *J. Am. Chem. Soc.* **1995**, *117*, 5179.
(43) Jorgensen, W. L.; Madura, J. D.; Swenson, C. L. *J. Am. Chem. Soc.* **1984**, *106*, 6638.
(44) Jorgensen, W. L.; Severance, D. L. *J. Am. Chem. Soc.* **1990**, *112*, 4768.
(45) Jorgensen, W. L.; Laird, E. R.; Nguyen, T. B.; Tirado Rives, J. *J. Comput. Chem.* **1993**, *14*, 206.
(46) Etchegoin, P. *Phys. Rev. E* **1997**, *56*, 538.
(47) Berendsen, H. J. C.; Postma, J. P. M.; van Gunsteren, W. F.; Di Nola, A.; Haak, J. R. *J. Chem. Phys.* **1984**, *81*, 3684.
(48) van Gunsteren, W. F.; Berendsen, H. J. C. *Angew. Chem.* **1990**, *102*, 1020.
(49) Hockney, R. W.; Eastwood, J. W. *Computer Simulations Using Particles*; McGraw-Hill: New York, 1981.
(50) Ryckaert, J. P.; Ciccotti, G.; Berendsen, H. J. C. *J. Comput. Phys.* **1977**, *23*, 327.
(51) Allen, M. P.; Tildesley, D. J. *Computer Simulation of Liquids*; Oxford University Press: Oxford, U.K., 1989.
(52) Ewald, P. P. *Ann. Phys.* **1921**, *64*, 253.
(53) Paschek, D.; Geiger, A. MOSCITO 3.9. Department of Physical Chemistry, University of Dortmund, 2000.
(54) Veillard-Baron, J. *Mol. Phys.* **1974**, *52*, 1303.
(55) Strandberg, K. J. In *Bond Orientational Order in Condensed Matter Systems*; Strandberg, K. J., Ed.; Springer: Berlin, 1992; Chapter 2.
(56) Engberts, E.; Berendsen, H. J. C. *J. Chem. Phys.* **1988**, *89*, 3718.